Journal of Molecular Histology (2018) 49:195–208
https://doi.org/10.1007/s10735-018-9759-2

ORIGINAL PAPER

Localization of epithelial sodium channel (ENaC) and CFTR in the germinal epithelium of the testis, Sertoli cells, and spermatozoa

Sachin Sharma[1] · **Aaron Hanukoglu**[2,3] · **Israel Hanukoglu**[1]

Received: 7 January 2018 / Accepted: 5 February 2018 / Published online: 16 February 2018

Abstract

Spermatogenesis starts within the seminiferous tubules of the testis by mitotic division of spermatogonia that produces spermatocytes. Meiotic division of these spermatocytes produces haploid spermatids that differentiate into spermatozoa. In this study, we examined the expression of ENaC and CFTR (a Cl^- channel) in rat testicular sections using confocal microscopic immunofluorescence. The structural integrity of the seminiferous tubule sections was verified by precise phalloidin staining of the actin fibers located abundantly at both basal and adluminal tight junctions. The acrosome forming regions in the round spermatids were stained using an FITC coupled lectin (wheat germ agglutinin). In all phases of the germ cells (spermatogonia, spermatocytes, and spermatids) ENaC was localized in cytoplasmic pools. Prior to spermiation, ENaC immunofluorescence appeared along the tails of the spermatids. In spermatozoa isolated from the epididymis, ENaC was localized at the acrosome and a central region of the sperm flagellum. The mature sperm are transcriptionally silent. Hence, we suggest that ENaC subunits in cytoplasmic pools in germ cells serve as the source of ENaC subunits located along the tail of spermatozoa. The locations of ENaC is compatible with a possible role in the acrosomal reaction and sperm mobility. In contrast to ENaC, CFTR immunofluorescence was most strongly observed specifically within the Sertoli cell nuclei. Based on the nuclear localization of CFTR we suggest that, in addition to its role as an ion channel, CFTR may have an independent role in gene regulation within the nuclei.

Keywords Acrosome · Actin · Blood-testis barrier · Ion channels · Parenchyma · Seminiferous tubule · Tubulin

Introduction

Spermatozoa develop from germ cells in the seminiferous tubules of the testis. This process starts with the mitotic division of the stem germ cells located adjacent to the basement membrane. The mitotic division results in two types of cells. Type A spermatogonia replenish the stem cells, and type B spermatogonia develop into spermatocytes that undergo meiotic division producing haploid spermatids that differentiate into mature spermatozoa (Rato et al. 2012; Chojnacka et al. 2016). During spermatogenesis, the germ cells are tightly connected to the Sertoli cells that form the main epithelium of the seminiferous tubules (França et al. 2016). Towards the end of the spermatogenesis, spermatozoa align in the lumen of the seminiferous tubule, develop a tail and are finally released from the Sertoli cell in a process called spermiation (O'Donnell et al. 2011). This process is repeated continuously in a cycle that has been named as the "cycle of the seminiferous epithelium" and total 14 stages in a cycle have been distinguished in rat seminiferous epithelium (Leblond and Clermont 1952; Dym and Clermont 1970).

A complex array of tight junctions that is called the "blood-testis barrier" (BTB) isolate the germ cells within the tubule and provide them an immune-privileged environment isolated from the circulatory and lymphatic systems (Mruk and Cheng 2015). These tight junctions

Electronic supplementary material The online version of this article (https://doi.org/10.1007/s10735-018-9759-2) contains supplementary material, which is available to authorized users.

✉ Israel Hanukoglu
mbiochem@gmail.com
https://www.science.co.il/hi/

[1] Laboratory of Cell Biology, Ariel University, 40700 Ariel, Israel

[2] Sackler Faculty of Medicine, Tel-Aviv University, Tel Aviv, Israel

[3] Division of Pediatric Endocrinology, E. Wolfson Medical Center, Holon, Israel

are located in between the Sertoli cells at the base of the tubules, and at the sites of contact between spermatids attached to Sertoli cells. At both locations, these junctions can be visualized by actin-binding stains as the tight junction scaffold that includes actin fibers (Li et al. 2016).

As a consequence of the BTB, the ionic and proteomic compositions of the seminiferous tubular fluid (STF) differ significantly from the interstitial fluid (Rato et al. 2010; Chalmel et al. 2014; Stanton et al. 2016). The STF provides the necessary milieu for developing spermatozoa and the medium to transport them into the epididymis. In both the STF and the interstitial fluid, the major cation is Na^+ (Rato et al. 2010). Yet, in the STF, the concentration of the K^+ ion is high relative to that in the serum (Rato et al. 2010). The concentration of these major electrolytes is a crucial determinant of the movement of fluid in the seminiferous tubules, as their differential concentrations across the semi-permeable membrane would lead to osmolarity differences. The expression and function of various ion pumps and channels (e.g. Na^+/K^+ ATPase, Na^+/H^+ exchanger, CFTR, Ca^{2+} channels) have been extensively studied in Sertoli cells (Rato et al. 2010; Alves et al. 2015). NHE3 a Na^+/H^+ exchanger knockout mice showed tubular fluid accumulation, testicular atrophy and associated infertility (Zhou et al. 2001). The sperm plasma membrane inherits specific ion channels and transporters that initiate the acrosomal reaction, and capacitation in sperm (Lishko et al. 2012; Beltrán et al. 2016). However, we could not locate any study providing high-resolution substantial evidence on the localization of epithelial sodium channel (ENaC) and cystic fibrosis transmembrane conductance regulator (CFTR) (a Cl^- channel) in the mammalian testis.

In a previous study, we documented the sites of expression of ENaC in the female reproductive tract (Enuka et al. 2012). In the present study, we examined the expression of both ENaC and CFTR in sections of rat testes. ENaC is composed of three homologous subunits (αβγ or δβγ) (Hanukoglu and Hanukoglu 2016; Hanukoglu 2017). To visualize ENaC channels we used an antibody against the α subunit. Previously, we had shown that the membrane expression of ENaC is dependent on all three subunits and that if one subunit is missing the level of ENaC expression on the cell surface is hardly detectable (Edelheit et al. 2011, 2014).

In this study, we show that in the spermatogonia, spermatocytes, and round spermatids ENaC is located in cytoplasmic stores. As the round spermatids transform into spermatozoa, ENaC location shifts from the cytoplasm to the tails. Relative to ENaC, the distribution of CFTR is limited. The strongest expression of CFTR was observed surprisingly in the nuclei of Sertoli cells. To the best of our knowledge, this is the first study demonstrating the localization of ENaC and CFTR in testis with high-resolution and specificity.

Materials and methods

Animals

Adult male Sprague Dawley strain rats, aged between 90 and 120 days, weighing around 300–350 g, were housed according to the standard laboratory conditions with ad libitum access to food and water. The testes were surgically removed immediately after CO_2 asphyxiation of the rats and processed separately for western blots and immunofluorescence as described below.

Antibodies and fluorescent tags

Rabbit polyclonal anti-ENaCα antisera against the extracellular domain of the α-subunit of human ENaC was generated in our lab. The specificity of the anti-ENaCα antisera against the ENaCα subunit was determined by tagged protein expression in an Sf9 insect cells culture system and verified by mass-spectral analysis (Enuka et al. 2012). The other antibodies and fluorescent tags we used are listed in Table 1.

Cryotomy and tissue sectioning

After tissue removal, the testes were immediately transferred to 4% w/v paraformaldehyde (BDH Limited Poole, England) in phosphate buffered saline (PBS) (10 mM potassium phosphate, pH 7.4 and 150 mM NaCl) and kept in this buffer for at least 24 h at 4 °C. The testes were then transferred to 30% w/v sucrose solution. After the tissues settled down at the bottom of the tube, the tissues were embedded in cryo-medium OCT compound (Tissue-Tek, Sakura, Netherlands), frozen, and stored at − 80 °C. Tissue blocks were then sliced into 25–30 µm thick sections on a cryostat (Leica Jung Frigocut 2000, Wetzlar, Germany) at − 25 °C and collected in PBS containing 0.1% sodium azide.

Immunofluorescence staining

The tissue slices were transferred into 24-well plates containing PBS. The PBS was then replaced with 4% PFA for 20 min fixation of the tissues. The samples were permeabilized in 0.1% Tween-20 (Sigma-Aldrich) in PBS for 10 min and washed three times with PBS for 5 min each. The samples were then blocked in 5% w/v bovine serum albumin (BSA) in PBS for 20 min and washed with PBS for 5 min. The primary antisera incubation was carried out at 4 °C overnight in PBS containing 2% BSA. The samples were washed six times in PBS (5 min each) and incubated

Table 1 Antibodies and fluorescent tags used in this study

Antibody/tag	Host, company, & catalog no.	Application—dilution
Anti-ENaCα	Rabbit In-house	IF—1:50 WB—1:1000
Anti-CFTR	Rabbit Alomone labs—#ACL-006	IF—1:100 WB—1:2000
Anti-α-tubulin	Mouse Millipore—#05-829	IF—1:500
Alexa Fluor 555 IgG (H + L)	Goat anti-rabbit Life technologies—#A21428	IF—1:200
Alexa Fluor 488 IgG (H + L)	Goat anti-mouse Life technologies—#A11029	IF—1:100
Peroxidase conjugate IgG (H + L)	Goat anti-rabbit Jackson immuno research—#111-035-003	WB—1:2000
CF488A conjugate phalloidin	Biotium # BTM-00042	IF—1:40
FITC conjugate WGA	Sigma-Aldrich—# L4895-2MG	IF—1:99

IF immunofluorescence, *WB* western blotting

with the secondary antibodies in PBS containing 2% BSA for 1 h. Immediately, the samples were washed six times for 5 min each.

The nuclei were counter-stained using DAPI (4′6-diamidino-2-phenylindole) for 2 min. Unless otherwise indicated, all the steps were carried out at room temperature. The samples were washed at least twice with PBS and then mounted onto X-tra adhesive slides (Leica Biosystems, Peterborough, UK) using the anti-fade reagent, n-propyl gallate (Sigma-Aldrich) in 100 mM phosphate buffer (pH 7.2).

To stain the actin filaments, tissue sections were incubated with CF488A phalloidin conjugate in PBS for 30 min either separately or immediately after the washing step of the secondary antibodies. The lectin binding sites were stained after incubating testis sections with FITC-WGA (wheat germ agglutinin) in PBS for 30 min. The flagella of the sperm were stained with anti-α-tubulin antisera.

For control experiments, the primary antiserum was replaced by either an antigen–antibody complex (competitive experiment) or omitted from the reactions. In such control slides, only DAPI (blue) staining was visible. All the experiments were performed at least three times with independent samples.

Isolation of sperm

The caudal part of the epididymis was isolated and thoroughly rinsed with PBS to remove blood contaminants and transferred into a petri dish filled with PBS. While the cauda was submerged in PBS, it was punctured at several sites using a 21-gauge needle causing the sperm to spill out into the petri dish. The sperm containing fluid was transferred using a pipette to a 15 ml tube. After 3 h at 4 °C, the upper layer containing motile sperm was aspirated and transferred to a 2 ml Eppendorf tube. The collected sperm were diluted in PBS for immunofluorescence studies. For immunofluorescence staining, a drop of this fluid was placed and allowed to dry on the slide.

Confocal microscopy

High-resolution fluorescent images were captured using an LSM 700 confocal microscope (Carl-Zeiss, Germany). The laser diodes used were 405 nm for excitation of DAPI, 488 nm for excitation of CF488A, FITC, and Alexa Fluor-488, and 555 nm for excitation of Alexa Fluor-555. Fluorescence and bright-field illumination modes were used during image acquisition process. Samples were visualized through EC Plan-Neofluar 10x/0.30 M27, LCI Plan-Apochromat 25x/0.8, EC Plan-Neofluar 40x/1.30, and Plan-Apochromat 63x/1.40 oil objective lenses. The composite images were generated using the tile-scan image overview mode and 3-D images were rendered by z-stack compilation.

Protein gel electrophoresis and western blots

Frozen tissue samples from rat kidney, lung, and testes were homogenized in 50 mM Tris–Cl (pH 7.4), 1 mM EDTA, and a protease inhibitor cocktail (Roche) at 4 °C. Tissue homogenates were briefly centrifuged to remove clumps and debris. The isolation of a nuclear fraction from the testis sample was carried out using the protocol of (Dimauro et al. 2012). The protein concentration of the tissue samples was measured using the Bradford method with BSA as a standard.

For electrophoresis, protein samples were dissolved in Laemmli sample buffer (50 mM Tris–HCl pH 6.8, 2% SDS, 0.2% bromophenol blue, 10% glycerol, and 5% β-mercaptoethanol), denatured at 98 °C for 5 min, and loaded onto an 8.5% polyacrylamide gel. After electrophoresis, the proteins were transferred onto a nitrocellulose

membrane (Bio-Rad) using a Bio-Rad apparatus. Initially, the membrane was blocked using 1% skimmed milk in PBS for 45 min at room temperature. The membrane was then incubated with either anti-ENaCα antisera for 3 h at room temperature or anti-CFTR antisera at 4 °C for overnight (12–14 h) in PBS containing 2% BSA. Afterwards, the membrane was washed four times in PBS-T (0.1% Tween-20 in PBS, 5 min each).

The membrane was then incubated with secondary antibody peroxidase-conjugated goat anti-rabbit IgG in freshly prepared PBS containing 2% BSA for 90 min at room temperature. The membrane was washed four times with 0.1% PBS-T for 5 min each. The peroxidase-labeled membrane was developed using a chemiluminescence method with luminol (Enuka et al. 2012). The membrane was soaked in 12 ml buffer containing 0.1 M Tris, pH 8.5, 2.5 mM luminol, 400 µm p-coumaric acid and 3 µl hydrogen peroxide. After 1 min, the membrane was dried on filter paper and visualized by ImageQuant LAS, 4000 mini (GE).

Results

Actin and lectin binding sites in the seminiferous tubules

Initially, to verify the structural integrity of the tissue sections and the spermatids, we stained the actin filaments using phalloidin and the acrosomal regions in developing spermatids using FITC-WGA that is a lectin that binds to complex carbohydrate moieties.

In the testis, the major sites of abundance of actin filaments are the basal and adluminal tight-junctions called ectoplasmic specializations (ES) (O'Donnell et al. 2000). Consistent with previous studies, the strong actin filament staining was observed with high precision at both basal and adluminal ES (Fig. 1). Since we used tile-scan imaging, Fig. 1 represents a much broader view of the actin filament distribution in a section that includes over 30 seminiferous tubules. In each tubule, high concentrations of actin

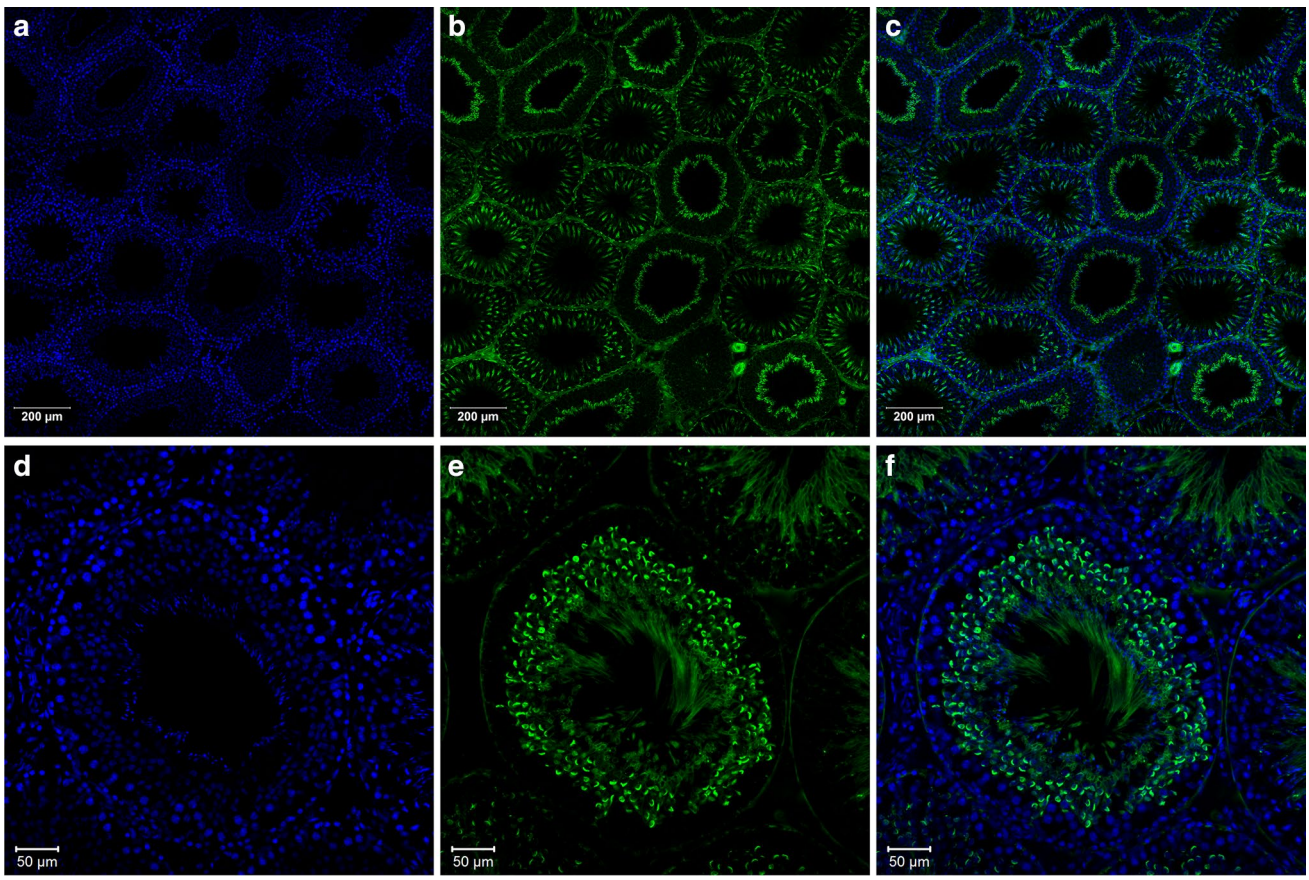

Fig. 1 Localization of actin filaments (**a**–**c**) and lectin binding sites (**d**–**f**) in the rat seminiferous tubules. A cross-section of a rat testis was reacted with: Top row **a** DAPI (blue) and **b** CF488A-phalloidin (green). Bottom row **d** DAPI (blue) and **e** FITC-WGA (green). In both rows, the rightmost image **c, f** shows the merged image of the first two images. Note that actin filaments were localized at basal and adluminal ectoplasmic specializations. The major lectin binding sites were observed in the round spermatids. Scale bars 200 µm for the top row and 50 µm for the bottom row. (Color figure online)

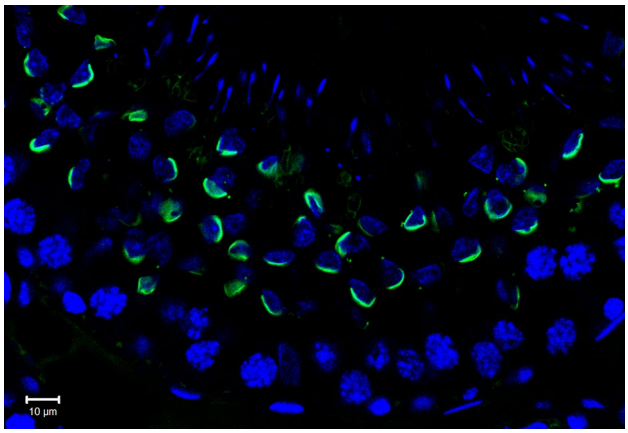

Fig. 2 A magnified view of the rat seminiferous tubule, focusing on the semicircular lectin binding sites in round spermatids. Note that the round spermatids are located in between two layers of (1) spermatocytes close to the basal membrane and (2) central layer of elongated spermatid nuclei. The lectin binding sites contain glycoproteins that are present in the acrosome of mature spermatozoa. Scale bar 10 µm

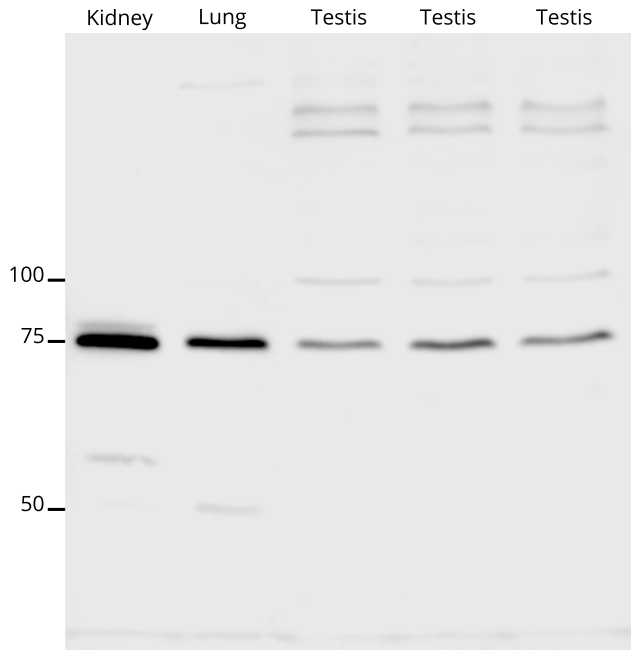

Fig. 3 Western blot analysis of total tissue protein from rat kidney, lung, and testis samples. Each lane was loaded with 75 µg of total protein. The testis samples were isolated from three different animals. The blot was reacted with anti-ENaCα antisera

filaments are localized at ES. The pattern of actin filament distribution manifests the stage of spermatogenesis in each seminiferous tubule (Fig. 1).

FITC conjugated WGA strongly stained the acrosomal regions of developing spermatids (Figs. 1f, 2). These results confirmed that our methods of processing of the tissue sections preserved the ultra-structure of the tissues and their normal physiology.

Western blot analysis of ENaC expression in the testis

The polyclonal anti-ENaCα antiserum we used was generated against the extracellular segment of the human ENaCα (Enuka et al. 2012). To confirm the specificity of this antibody in the rat tissues, we reacted western blots containing total protein from rat kidney, lung, and testis with the anti-ENaCα antibody. In all tissues, the antibody detected the expected major band of ~ 75 kDa and a few additional faint bands (Fig. 3). The higher MW bands represent glycosylated subunits (Hanukoglu et al. 2017), and the ~ 50 kDa band represents a processed subunit (Fig. 3) (Hanukoglu and Hanukoglu 2016). The ~ 50 kDa processed subunit was observed previously in both kidney and lung samples (Enuka et al. 2012). However, we could not see a trace of a similarly processed subunit in the testis samples from rats (Fig. 3). Kong et al. reported a single band of ~ 75 kDa not only in rat testis but also in kidney extracts (Kong et al. 2009). The difference between our observations as opposed to Kong's results may be due to the fact that we carried out western blot analysis using total tissue protein, whereas Kong et al. carried out their analysis on plasma membrane samples isolated using a membrane protein extraction kit (Kong et al. 2009).

Localization of ENaC in the seminiferous tubules

In rat testis sections, ENaC immunofluorescence was detected within all the seminiferous tubules but not in the interstitial cells (Fig. 4). In the control experiments, anti-ENaCα antisera was omitted from the reactions. These slides did not show ENaC staining, indicating compatibility of anti-ENaCα antisera (Supplementary Fig. 1). A seminiferous tubule includes the germinal epithelium with cells at different stages of development and the Sertoli cells that encompass these germ cells. Below we present the expression profiles of ENaC in these cell types separately.

Germ cells

Spermatozoa develop from the reservoir of stem germ cells located beneath the basal lamina of the seminiferous tubules. These germ cells undergo tightly regulated events of mitotic and meiotic cell divisions, to replenish the reservoir of stem germ cells and to produce haploid spermatozoa. The architecture of seminiferous tubule sections varies depending upon the stage of the seminiferous epithelium cycle.

Figure 5 shows ENaC immunofluorescence in two tubules at different stages of the spermatogenesis.

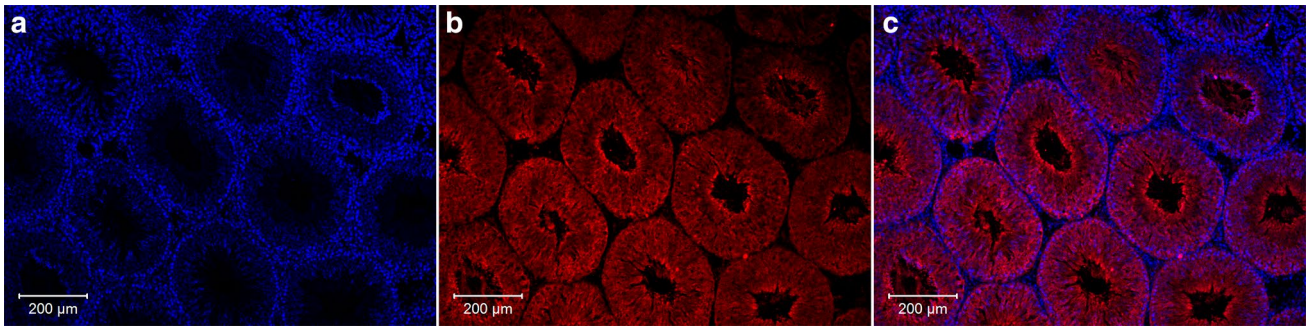

Fig. 4 Localization of ENaC in the rat seminiferous tubules. A testis section was reacted with DAPI and anti-ENaCα antisera as described in "Materials and methods". **a** Blue-colored DAPI staining of cell nuclei. **b** Anti-ENaCα immunofluorescence. **c** Merged image of **a** and **b**. Note that, all seminiferous tubules stained uniformly with anti-ENaCα antisera. The interstitial cells were only stained with DAPI and showed only isolated spots of weak red fluorescence. Scale bar 200 µm. (Color figure online)

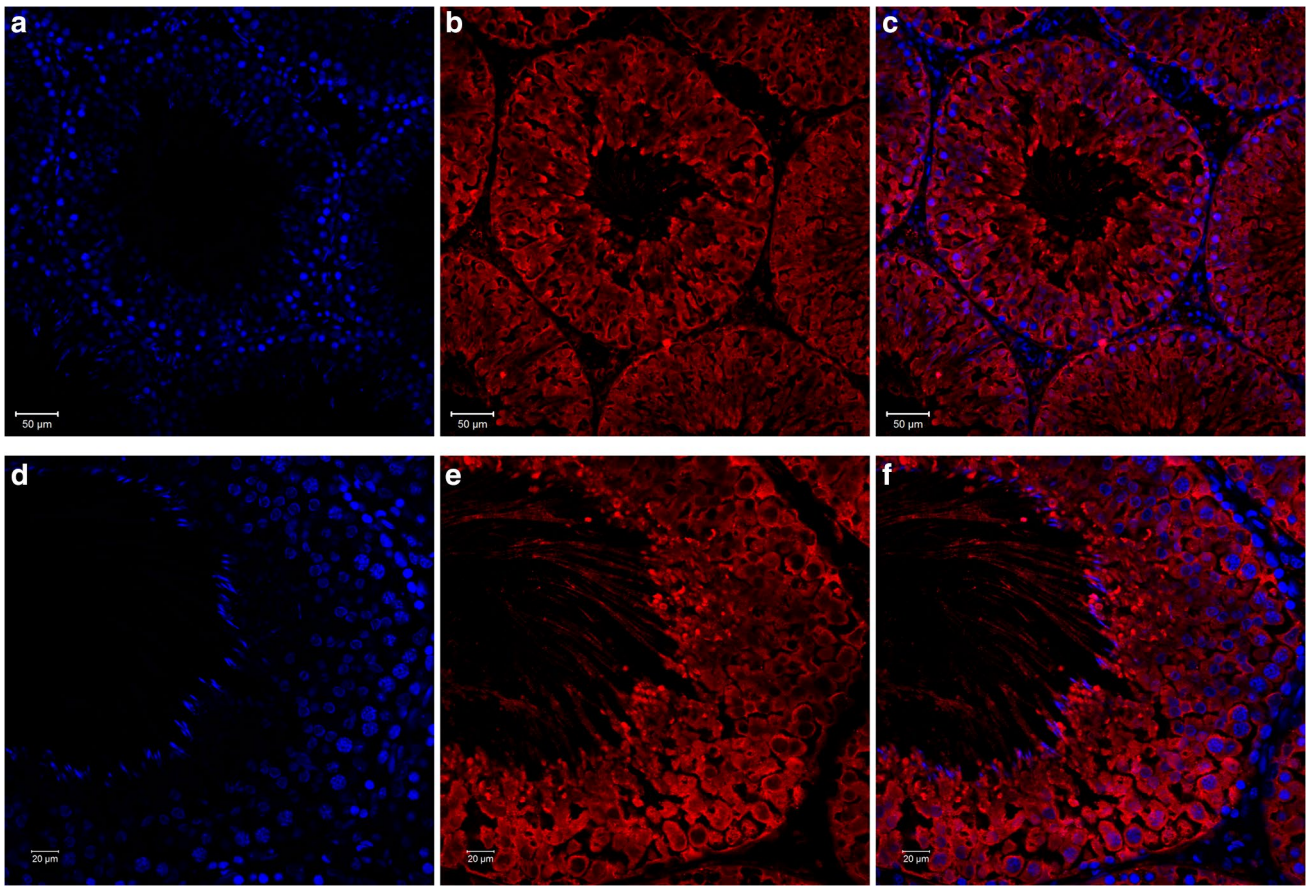

Fig. 5 Expression of ENaC in two seminiferous tubules at different stages of spermatogenesis. **a** and **d** DAPI staining of cell nuclei (blue); **b** and **e** Anti-ENaCα immunofluorescence (red); and **c** and **f** Merged images. Scale bars 50 µm for the images on top and 20 µm for those below. (Color figure online)

(Leblond and Clermont 1952). There is a major difference in the ENaC immunofluorescence between these two stages (Fig. 5b, e). In the tubule at upper row, ENaC immunofluorescence appears in all the cells (Fig. 5b). In the lower row, in addition to cytoplasmic localization, ENaC immunofluorescence appears along the thin tails of the spermatids that whirl in the center of tubule (Fig. 5e). In the merged image, it can be seen that the tails start at the base of the spermatid nuclei and extend into the lumen of the tubule (Fig. 5f). The interstitial spaces around the

tubules show nuclear DAPI staining and either very weak or no anti-ENaCα staining (Fig. 5c, f).

Figure 6 shows a magnified view of two adjacent seminiferous tubules. The germ cells can be identified by their round nuclear shape and strong DAPI staining as compared to the Sertoli cells nuclei. In all of these cells, ENaC immunofluorescence is observed within the cytoplasm and outside of the DAPI stained nuclear region (Fig. 6). Actin filament staining (green) can be easily identified in two patterns: (1) Short stretches of actin filaments parallel to the basal membrane that mark the basal ES; and (2) long stretches of actin overlapping with the elongated nuclei that mark the adluminal ES (Fig. 6b). Note that the basal ES appears between the borders of the germ cells and the Sertoli cells at the basal region in the seminiferous tubules (Fig. 6d). The major function of these actin filaments is to anchor the molecules that are responsible for the tight-junctions framework in the seminiferous epithelium.

Sertoli cells

Sertoli cells represent an essential scaffold for the development of spermatozoa (França et al. 2016). Thus, we paid particular attention to identify Sertoli cells in the seminiferous tubule sections. Leblond and Clermont (1952) had described that Sertoli cell nuclei differ from the nuclei of germ cells

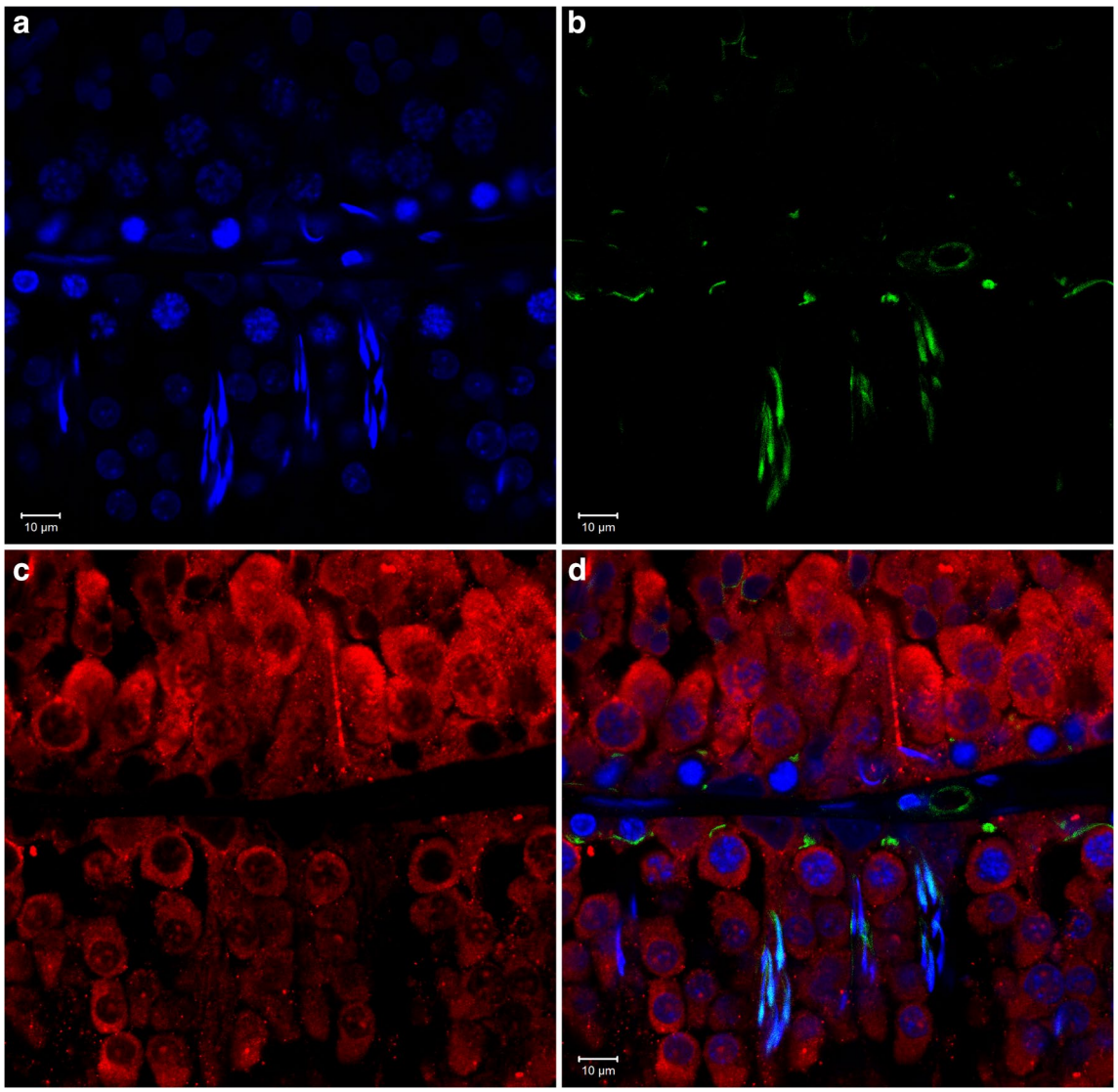

Fig. 6 A magnified view of two adjacent seminiferous tubules showing the sites of localization of ENaC and actin filaments. **a** DAPI staining of cell nuclei (blue); **b** CF488A-phalloidin fluorescence (green); **c** anti-ENaCα immunofluorescence (red); and **d** merged image of **a, b**, and **c**. Note that ENaC immunofluorescence was observed only in the *cytoplasmic region* of the cells. The *peritubular myoid cells* that are characterized by the elongated nuclei (in between the two tubules) did not show ENaC immunofluorescence. A small circular region of actin staining may represent a blood vessel. Scale bar 10 µm. (Color figure online)

and can be grouped into two types based on their shape in cross section: (1) Flat or oval nuclei that are located in parallel to the basement membrane of the tubule. (2) Triangular or oblong nuclei that have the longer axis perpendicular to the basement membrane. In addition, Sertoli cells are highly euchromatic (França et al. 2016) and as compared to germ cells stain weakly with DAPI. Using these two characteristics we identified Sertoli cell nuclei.

In a magnified view of the border of two neighboring tubules, several Sertoli cell nuclei could be easily identified by their location near to the basement membrane, characteristic triangular shapes, and much weaker DAPI staining relative to germ cells (Fig. 6a). Moreover, in the lower row of Fig. 6, immature spermatids that are embedded in Sertoli cells could be identified by their very strong DAPI staining and particular shapes of elongated spermatid nuclei (Fig. 6). In most cases shown in Fig. 6 and other sections, we consistently observed ENaC immunofluorescence that extends from the top border of the Sertoli cell nuclei and towards the lumen. Thus, based on these observations it appears that ENaC is also expressed in Sertoli cells.

Peritubular myoid cells

The outermost layer of the seminiferous tubules includes peritubular myoid cells that are responsible for maintaining the structural integrity of the tubules (Potter and DeFalco 2017). The nuclei of myoid cells have an elongated shape that can be recognized at the outer edge of seminiferous tubules (Fig. 6). The area surrounding these nuclei are devoid of ENaC immunofluorescence (Fig. 6). Thus, it appears that ENaC is not expressed in these cells. The border region between the tubules also includes interstitial cells that show no ENaC immunofluorescence (Fig. 6).

Localization of ENaC on the sperm head and tail

As noted above, in some tubules ENaC immunofluorescence was detected along the flagella of the spermatozoa hanging in the lumen (Fig. 5e). To further examine the localization of ENaCα on mature sperm, samples were isolated from the caudal part of the epididymis.

The heads and the flagella of sperms were specifically stained using DAPI and anti-α-tubulin antibody respectively (Supplementary Fig. 2). The secondary antibody (Alexa Fluor 555 IgG) alone did not yield any immunofluorescence (Supplementary Fig. 2c).

When sperm were co-incubated with anti-α-tubulin and anti-ENaCα antisera together, ENaC immunofluorescence was observed on the mid-region of the principal-piece of the flagellum (Fig. 7). The site of localization of ENaCα begins at a distance of ~ 70 µm from the bottom of the sperm nucleus and continues for a span of ~ 60 µm along the flagellum. In a magnified view at the principal-piece of the flagellum, ENaC immunofluorescence was observed on both flanks associated with the plasma membrane enveloping the microtubules (Fig. 7c, inset).

To further confirm the precise location of anti-ENaC binding we examined immunofluorescence in a z-stack containing six slices. This three-dimensional image clearly indicated that ENaC is localized on top of sperm nuclei (acrosome), and the mid-piece of the sperm tail surrounding the microtubule (Fig. 8). This reinforces the evidence for membranous localization of ENaC in the sperm flagellum.

Sub-cellular localization of CFTR in the seminiferous tubules

Figure 9b, c show CFTR immunofluorescence (red) in two seminiferous tubules of the rat testis. The CFTR immunofluorescence appears most strongly in cells located in parallel to the basement membrane (Fig. 9c). In a supplementary figure, we present a tile-scan image showing a section with a much larger view including about sixteen seminiferous tubules with the same pattern of CFTR expression (Supplementary Fig. 3).

We could not detect any CFTR immunofluorescence in a control experiment, where the tissue slice was reacted with the anti-CFTR antiserum that was pre-incubated with the CFTR antigen control peptide (Fig. 9e). Figure 9f is a merged image that shows only DAPI staining without any CFTR staining. This control experiment provided further evidence for the specificity of the anti-CFTR antiserum.

Figure 10 shows a magnified view of the border region of two adjacent tubules. In the merged image (Fig. 10c) the red CFTR immunofluorescence and the blue DAPI staining are overlapping (Fig. 10c).

Leblond and Clermont (1952) described the shape of the nuclei of Sertoli cells. Sertoli cell nuclei are highly euchromatic and stain weakly with DAPI as compared to the germ cell nuclei. The shape of the nuclei showing CFTR immunofluorescence match these descriptions and characteristics (Figs. 9, 10). Thus, the pattern of strong CFTR immunofluorescence clearly indicates that CFTR is mostly localized in the nuclei of the Sertoli cells.

Since this finding of CFTR in the nucleus was surprising, we tested an independent batch of anti-CFTR antisera and obtained identical results of very high immunofluorescence in Sertoli cell nuclei.

Western blot analysis

In western blots of total testis tissue protein, we observed multiple bands in all samples from the lung and testis. CFTR is a highly glycosylated protein and its post-translational modifications yield multiple bands in western

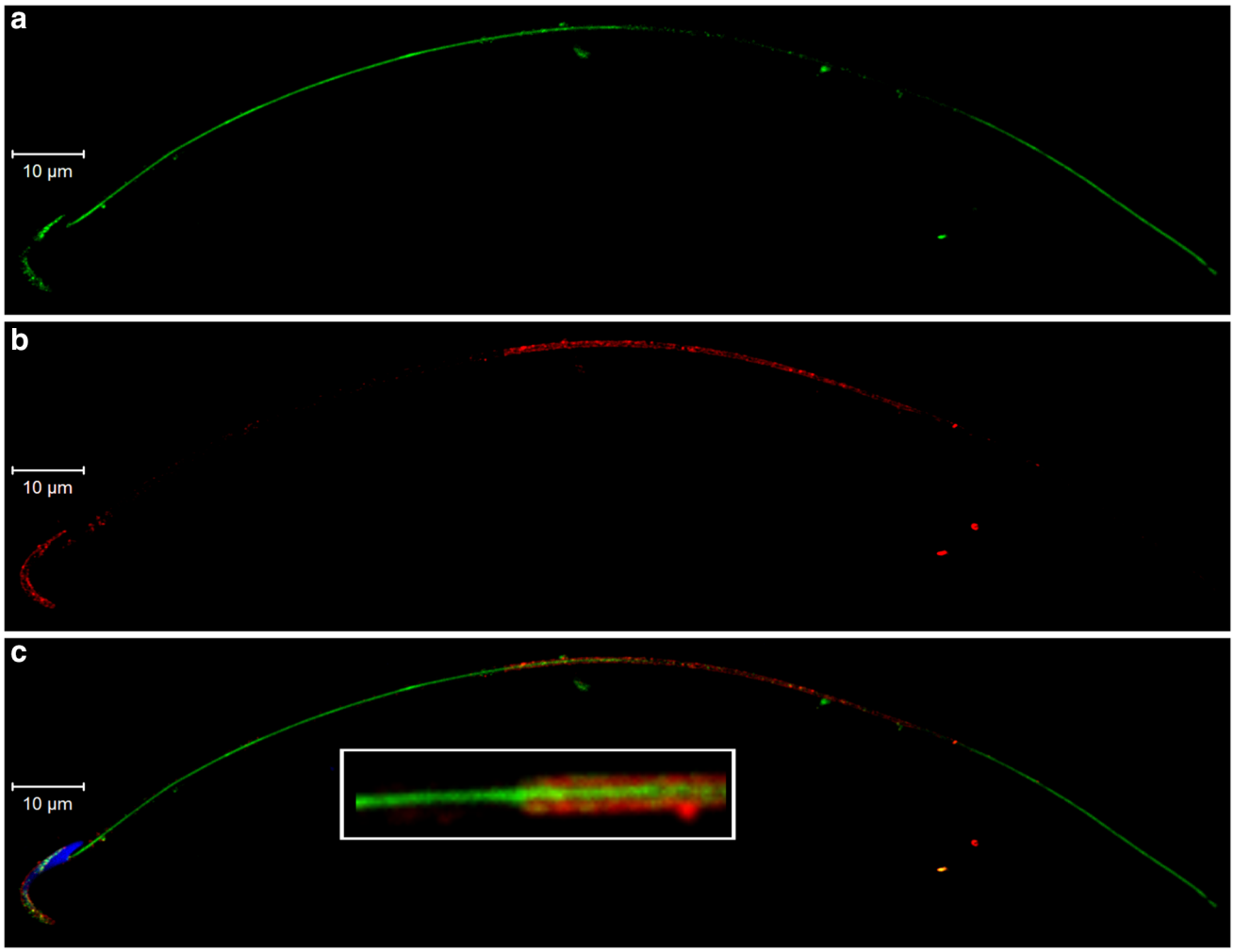

Fig. 7 Localization of ENaC and α-tubulin in mature rat sperm isolated from the caudal part of the epididymis. The sperm were reacted with: **a** Anti-α-tubulin antisera (green), **b** Anti-ENaCα antisera (red), and **c** DAPI (blue) (merged image). The α-tubulin antisera stained the sperm flagellum. The ENaC immunofluorescence (red) was observed at acrosome region of the sperm head and the principal-piece of the sperm flagellum. Inset in **c** A magnified view showing that ENaC subunits (red) are located on both the sides of the central microtubules (green). Scale bar 10 µm. (Color figure online)

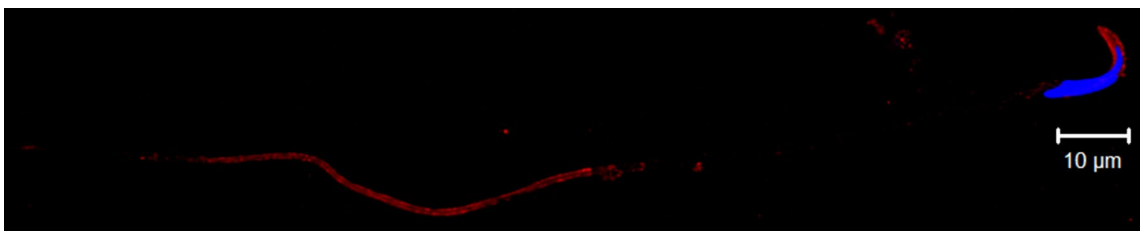

Fig. 8 Localization of ENaC in a 3D image of rat sperm. The sperm were reacted with DAPI (blue) and anti-ENaCα antisera (red). A 3D image was rendered from a z-stack performed on the sperm sample. ENaC immunofluorescence was specifically localized at the tip of the hook-like shape of a rat nucleus where acrosome is located. Scale bar 10 µm. (Color figure online)

blots, usually known as bands A, B, and C (Painter et al. 2006; Sorio et al. 2011). In rat lung and testis samples, the strongest band was observed at ~ 120 kDa (Fig. 11). Bands A (~ 100 kDa) and C (~ 160 kDa) showed lower intensities (Fig. 11). In the experiment shown in Fig. 11, and in additional experiments we carried out with independent testis samples, we observed similar patterns of stained bands among different rats.

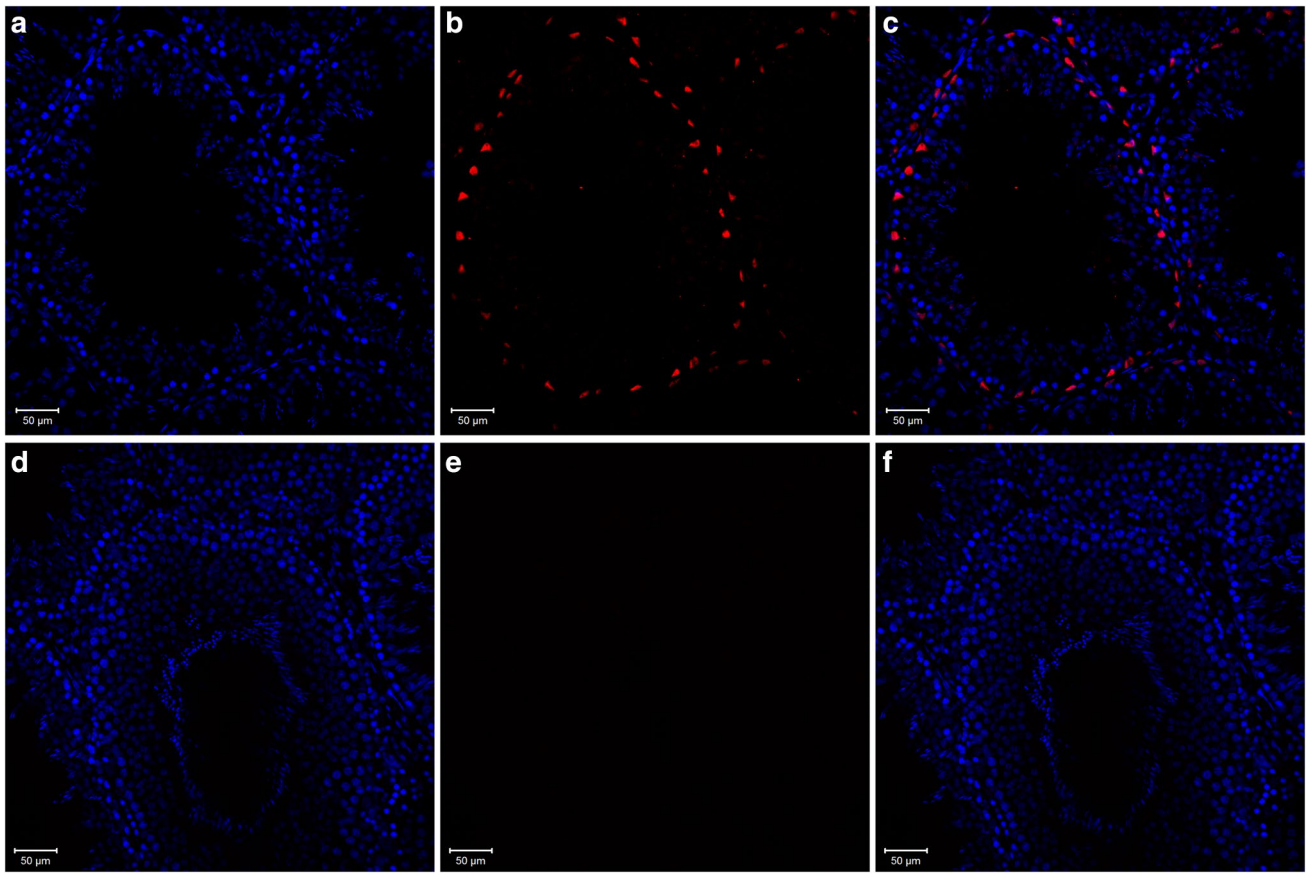

Fig. 9 Localization of CFTR in rat seminiferous tubules. **a** and **d** DAPI staining of cell nuclei (blue); **b** anti-CFTR immunofluorescence (red), **e** control immunofluorescence with anti-CFTR antisera pre-incubated with CFTR antigen; and **c** and **f** merged images. Note that strong CFTR immunofluorescence (red) was observed only in cells adjacent to the basal lamina of the seminiferous tubule. In the control slide **e** no red fluorescence of CFTR was observed, indicating the specificity of the reaction. Scale bar 50 µm. (Color figure online)

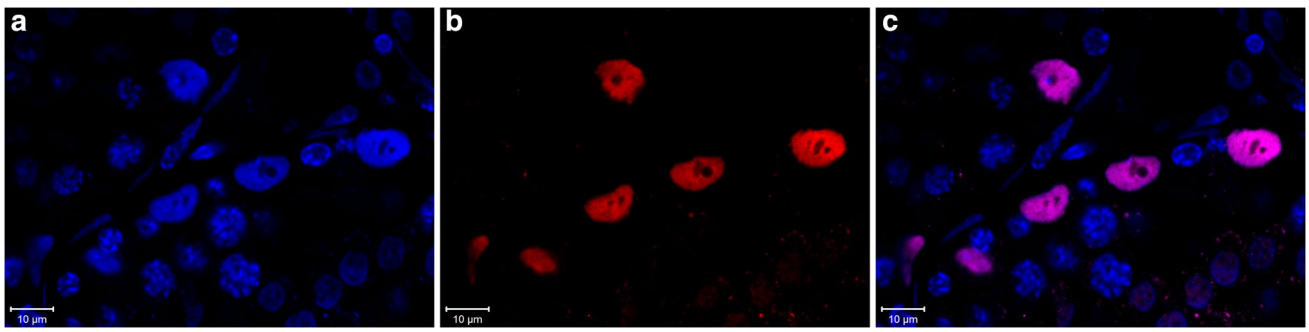

Fig. 10 A magnified view of the basal laminal region of two adjacent seminiferous tubules. Note that the blue DAPI staining was co-localized with red CFTR immunofluorescence showing the nuclear localization of CFTR. The characteristic shape of the nuclei indicates that CFTR is localized in the nuclei of the Sertoli cells. Scale bar 10 µm. (Color figure online)

As noted above, in immunofluorescence confocal microscopy, CFTR was observed in the nuclei of the Sertoli cells. To cross-check our findings, we performed a subcellular fractionation of total testis tissue homogenates as described in the "Materials and methods" section. After this fractionation, the nuclear fraction showed a very strong band at ~ 85 kDa (Fig. 11). The same ~ 85 kDa band was also observed in the total testis protein samples but at a lower intensity (Fig. 11). However, the (post-nuclear) supernatant fraction did not show this band. The nuclear fraction sample contained only 10 µg of total protein amount as compared to other samples that had 75 µg of total protein. These results

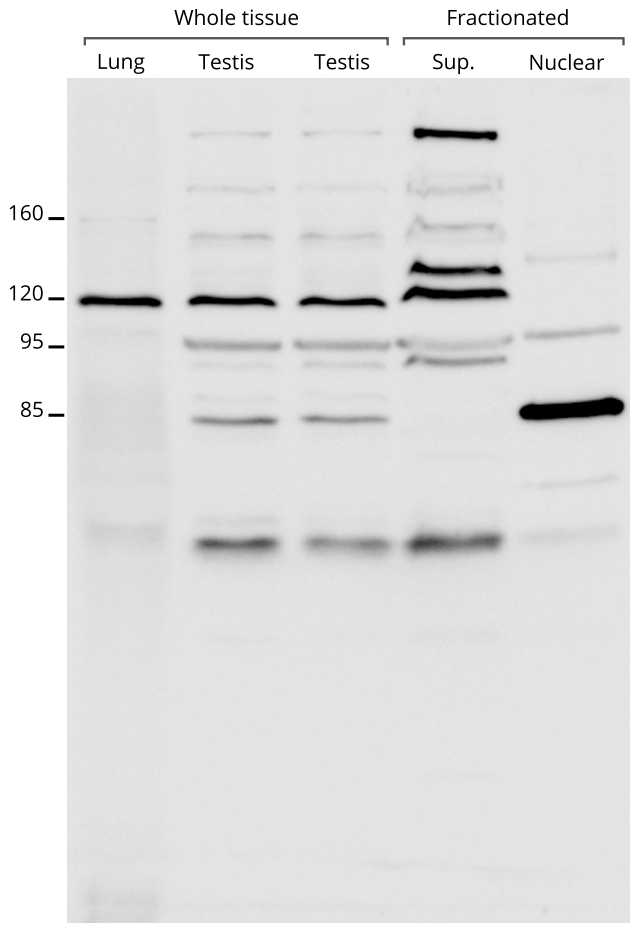

Fig. 11 Western blot analysis of total protein from rat lung and testis tissue homogenates, and subcellular fractions from testis homogenates. *Sup* post-nuclear supernatant. *Nuclear* nuclear fraction isolated as described in "Materials and methods". The blot was reacted with the anti-CFTR antibody. Total protein loaded in the first four lanes was 75 µg. Total protein loaded in the nuclear fraction lane was 10 µg. The numbers on the left side of the figure indicate the MWs of the observed major bands

establish that the protein that binds the anti-CFTR antibody is strongly concentrated in the nuclear fraction, consistent with the confocal microscopy results (Fig. 9).

Discussion

In this study, we examined the sites of localization of ENaC and CFTR in the rat testis. ENaC, as a sodium channel, and CFTR as a chloride transporter fulfill coordinated functions in many types of epithelia, the best known of which is the lung epithelia that is affected in cystic fibrosis patients and also systemic (multi-system) pseudohypoaldosteronism (PHA) patients (Hanukoglu et al. 1994; Collawn et al. 2012). Below we discuss our major findings in the light of our current knowledge in this field.

Expression and function of ENaC

In most mammals, ENaC is a non-voltage gated sodium channel that is composed of three subunits in an αβγ or δβγ configuration (Hanukoglu and Hanukoglu 2016; Hanukoglu 2017). The gene coding for the delta subunit apparently has been lost in the rat and mouse genomes (Giraldez et al. 2012; Hanukoglu and Hanukoglu 2016). Since the Na^+ ion is the major electrolyte in extracellular fluids, modulation of its concentration by ion channels can greatly affect trans-cellular fluid movement and consequently cellular volume. The major blood volume and blood pressure regulatory actions of ENaC are mediated by the αβγ trimer, and so far no involvement of the delta subunit has been reported in hereditary syndromes associated with ENaC mutations (Hanukoglu and Hanukoglu 2016). The expression of the delta ENaC subunit was shown by Northern blot analysis of the human testis mRNA (Waldmann et al. 1995). However, this approach could not distinguish between the type of cells where ENaC is expressed in the testis. A study on mouse sperm presented evidence for the expression of ENaCα and -δ subunits using PCR and immunostaining (Hernández-González et al. 2006). However, the results of this study on the expression of the δ subunit have been questioned as "nonspecific binding" as the mouse genome does not have a functional gene that codes for the delta subunit (Giraldez et al. 2012).

The electro-physiological experiments performed in this study provided evidence that ENaC participates in the regulation of the mouse sperm capacitation. A later study showed expression of ENaCα in the human and rat testis and spermatozoa (Kong et al. 2009). However, results of this study had poor resolution and localization of ENaC channel was not visualized in tissue sections.

Our results show that ENaCα is expressed throughout the differentiation of germ cells from the stage of spermatogonia to the stage of spermatids. However, the localization of ENaC changes during these developmental stages. The mature sperm are transcriptionally silent (Baker 2011). Therefore, most of the proteins that are required for the proper functioning of spermatozoa have to be synthesized prior to spermiation. There is evidence that in spermatozoa, nuclear-encoded mRNAs may be translated by the mitochondrial translational system (Gur and Breitbart 2006). However, this process is limited to a small number of proteins (Baker 2011). Therefore, we suggest that the ENaC subunits that are initially located in cytoplasmic pools in germ cells, serve as the source of the ENaC subunits that end up at acrosomal region and plasma membrane of the principal-piece of the sperm.

Previous studies on other Na^+ ion channels and transporters have demonstrated that regulation of Na^+ ion fluxes is critical for the processes of spermatogenesis, acrosomal reaction and sperm fertility (Rato et al. 2010; Beltrán et al.

2016). Currently, we do not know whether ENaC is essential for spermatogenesis and fertility. Transgenic mice with inactivation of the SCNN1A, SCNN1B, or SCNN1G genes that code for the α, β, and γ subunits have been produced. But, these mice die within a few days after birth (Bonny and Hummler 2000), so it has not been possible to assess the effect of gene-knockout on fertility of these mice.

In humans, mutations in SCNN1A, SCNN1B, and SCNN1G genes have been shown to be responsible for systemic PHA (Chang et al. 1996; Edelheit et al. 2005; Hanukoglu and Hanukoglu 2016). Our previous studies provided evidence that a functional ENaC is essential for normal female reproductive function (Hanukoglu et al. 2008; Enuka et al. 2012). None of the male PHA patients, known to us, have married yet. Therefore, we do not know whether the mutations they have in ENaC genes may affect their fertility.

Expression and function of CFTR

CFTR is a cAMP-dependent Cl^- channel that is encoded by the CFTR gene (UniProt code: CFTR_RAT). CFTR is generally located on the apical membrane of epithelia such as the respiratory tract, and eccrine sweat glands (Kreda et al. 2005; Enuka et al. 2012; Hanukoglu et al. 2017). Various studies suggest that CFTR might be coupled spatially or temporally to a wide array of partners including ion channels, receptors, transporters, scaffolding proteins, enzymes and signaling molecules creating a plasticity of interactions (Li and Naren 2010).

The expression of CFTR in rat Sertoli cells was shown first by RT-PCR, western blot analysis, and in functional assays (Boockfor et al. 1998). Our results revealed that CFTR immunofluorescence is most strongly concentrated in the nuclei of Sertoli cells (Fig. 9). Testis tissue sections reacted with anti-CFTR antisera that was pre-incubated with the control antigen, showed no CFTR immunofluorescence, providing further evidence for the specificity of the CFTR reaction in the testis sections.

Since the results showing a nuclear concentration of CFTR was surprising, we undertook an independent examination of the nuclear localization using western blot analysis of subcellular fractions (Fig. 11). The nuclear fraction of the testis homogenate exhibited a high-intensity band at ~85 kDa, that was present only weakly in the total tissue homogenate (Fig. 11). These findings support the hypothesis that a processed fragment of CFTR is concentrated in the nucleus as we observed in the immunofluorescence studies.

The observation that CFTR is located in Sertoli cell nuclei suggests that in addition to its function as an ion channel, CFTR may have an independent role in gene regulation within nuclei. We are raising this hypothesis in view of the decades-long speculations to understand the mechanism(s) by which cystic fibrosis causing mutations also result in a variety of abnormalities that lead to male infertility. Mutations in CFTR have been shown to be associated with reduced quantity and quality of sperm, azoospermia, and congenital bilateral absence of the vas deferens (Chen et al. 2012; Chan 2013; Fok et al. 2014; Jiang et al. 2017). Examination of the hypothesis for a nuclear role of CFTR will involve further extensive work.

In conclusion, based on our observations on CFTR expression specifically in Sertoli cell nuclei, we suggest that additional mechanisms of action should be sought for CFTR in the regulation of gene expression in the male reproductive system.

Acknowledgements This research was funded in part by a grant from the United States-Israel Bi-national Science Foundation (BSF Grant Number 2011370).

Compliance with ethical standards

Conflict of interest The authors have no conflict of interest that could be perceived as prejudicing the impartiality of the research reported.

References

Alves MG, Sá R, Jesus TT, Sousa M, Oliveira PF (2015) CFTR regulation of aquaporin-mediated water transport: a target in male fertility. Curr Drug Targets 16:993–1006

Baker MA (2011) The'omics revolution and our understanding of sperm cell biology. Asian J Androl 13:6–10. https://doi.org/10.1038/aja.2010.62

Beltrán C, Treviño CL, Mata-Martínez E, Chávez JC, Sánchez-Cárdenas C, Baker M, Darszon A (2016) Role of ion channels in the sperm acrosome reaction. In: Advances in anatomy, embryology, and cell biology. Springer, New York, pp 35–69

Bonny O, Hummler E (2000) Dysfunction of epithelial sodium transport: from human to mouse. Kidney Int 57:1313–1318. (https://doi.org/10.1046/j.1523-1755.2000.00968.x)

Boockfor FR, Morris RA, DeSimone DC, Hunt DM, Walsh KB (1998) Sertoli cell expression of the cystic fibrosis transmembrane conductance regulator. Am J Physiol 274:C922–C930

Chalmel F, Com E, Lavigne R, Hernio N, Teixeira-Gomes A-P, Dacheux J-L, Pineau C (2014) An integrative omics strategy to assess the germ cell secretome and to decipher sertoli-germ cell crosstalk in the Mammalian testis. PLoS ONE 9:e104418. https://doi.org/10.1371/journal.pone.0104418

Chan HC (2013) CFTR and male fertility—impact beyond cystic fibrosis. Spermatogenesis 3:e26228. https://doi.org/10.4161/spmg.26228

Chang SS, Grunder S, Hanukoglu A, Rösler A, Mathew PM, Hanukoglu I, Schild L, Lu Y, Shimkets RA, Nelson-Williams C et al (1996) Mutations in subunits of the epithelial sodium channel cause salt wasting with hyperkalaemic acidosis, pseudohypoaldosteronism type 1. Nat Genet 12:248–253. https://doi.org/10.1038/ng0396-248

Chen H, Ruan YC, Xu WM, Chen J, Chan HC (2012) Regulation of male fertility by CFTR and implications in male infertility. Hum Reprod Update 18:703–713. https://doi.org/10.1093/humupd/dms027

Chojnacka K, Zarzycka M, Mruk DD (2016) Biology of the sertoli cell in the fetal, pubertal, and adult mammalian testis. Results

Probl Cell Differ 58:225–251. https://doi.org/10.1007/978-3-319-31973-5_9
Collawn JF, Lazrak A, Bebok Z, Matalon S (2012) The CFTR and ENaC debate: how important is ENaC in CF lung disease? Am J Physiol Lung Cell Mol Physiol 302:L1141–L1146. https://doi.org/10.1152/ajplung.00036.2012
Dimauro I, Pearson T, Caporossi D, Jackson MJ (2012) A simple protocol for the subcellular fractionation of skeletal muscle cells and tissue. BMC Res Notes 5:513. https://doi.org/10.1186/1756-0500-5-513
Dym M, Clermont Y (1970) Role of spermatogonia in the repair of the seminiferous epithelium following X-irradiation of the rat testis. Am J Anat 128:265–281. https://doi.org/10.1002/aja.1001280302
Edelheit O, Hanukoglu I, Gizewska M, Kandemir N, Tenenbaum-Rakover Y, Yurdakök M, Zajaczek S, Hanukoglu A (2005) Novel mutations in epithelial sodium channel (ENaC) subunit genes and phenotypic expression of multisystem pseudohypoaldosteronism. Clin Endocrinol 62:547–553. https://doi.org/10.1111/j.1365-2265.2005.02255.x
Edelheit O, Hanukoglu I, Dascal N, Hanukoglu A (2011) Identification of the roles of conserved charged residues in the extracellular domain of an epithelial sodium channel (ENaC) subunit by alanine mutagenesis. Am J Physiol Renal Physiol 300:F887–F897. https://doi.org/10.1152/ajprenal.00648.2010
Edelheit O, Ben-Shahar R, Dascal N, Hanukoglu A, Hanukoglu I (2014) Conserved charged residues at the surface and interface of epithelial sodium channel subunits—roles in cell surface expression and the sodium self-inhibition response. FEBS J 281:2097–2111. https://doi.org/10.1111/febs.12765
Enuka Y, Hanukoglu I, Edelheit O, Vaknine H, Hanukoglu A (2012) Epithelial sodium channels (ENaC) are uniformly distributed on motile cilia in the oviduct and the respiratory airways. Histochem Cell Biol 137:339–353. https://doi.org/10.1007/s00418-011-0904-1
Fok KL, Chen H, Ruan YC, Chan HC (2014) Novel regulators of spermatogenesis. Semin Cell Dev Biol 29:31–42. https://doi.org/10.1016/j.semcdb.2014.02.008
França LR, Hess RA, Dufour JM, Hofmann MC, Griswold MD (2016) The sertoli cell: one hundred fifty years of beauty and plasticity. Andrology 4:189–212. https://doi.org/10.1111/andr.12165
Giraldez T, Rojas P, Jou J, Flores C, Alvarez de la Rosa D (2012) The epithelial sodium channel δ-subunit: new notes for an old song. Am J Physiol Renal Physiol 303:F328-F338. https://doi.org/10.1152/ajprenal.00116.2012
Gur Y, Breitbart H (2006) Mammalian sperm translate nuclear-encoded proteins by mitochondrial-type ribosomes. Genes Dev 20:411–416. https://doi.org/10.1101/gad.367606
Hanukoglu I (2017) ASIC and ENaC type sodium channels: conformational states and the structures of the ion selectivity filters. FEBS J 284:525–545. https://doi.org/10.1111/febs.13840
Hanukoglu I, Hanukoglu A (2016) Epithelial sodium channel (ENaC) family: phylogeny, structure-function, tissue distribution, and associated inherited diseases. Gene 579:95–132. https://doi.org/10.1016/j.gene.2015.12.061
Hanukoglu A, Bistritzer T, Rakover Y, Mandelberg A (1994) Pseudohypoaldosteronism with increased sweat and saliva electrolyte values and frequent lower respiratory tract infections mimicking cystic fibrosis. J Pediatr 125:752–755. (https://doi.org/10.1016/S0022-3476(06)80176-9)
Hanukoglu A, Edelheit O, Shriki Y, Gizewska M, Dascal N, Hanukoglu I (2008) Renin-aldosterone response, urinary Na/K ratio and growth in pseudohypoaldosteronism patients with mutations in epithelial sodium channel (ENaC) subunit genes. J Steroid Biochem Mol Biol 111:268–274. https://doi.org/10.1016/j.jsbmb.2008.06.013
Hanukoglu I, Boggula VR, Vaknine H, Sharma S, Kleyman T, Hanukoglu A (2017) Expression of epithelial sodium channel (ENaC) and CFTR in the human epidermis and epidermal appendages. Histochem Cell Biol 147:733–748. https://doi.org/10.1007/s00418-016-1535-3
Hernández-González EO, Sosnik J, Edwards J, Acevedo JJ, Mendoza-Lujambio I, López-González I, Demarco I, Wertheimer E, Darszon A, Visconti PE (2006) Sodium and epithelial sodium channels participate in the regulation of the capacitation-associated hyperpolarization in mouse sperm. J Biol Chem 281:5623–5633. https://doi.org/10.1074/jbc.M508172200
Jiang L, Jin J, Wang S, Zhang F, Dai Y, Shi L, Zhang S (2017) CFTR gene mutations and polymorphism are associated with non-obstructive azoospermia: from case-control study. Gene 626:282–289. https://doi.org/10.1016/j.gene.2017.04.044
Kong X-B, Ma H-G, Li H-G, Xiong C-L (2009) Blockade of epithelial sodium channels improves sperm motility in asthenospermia patients. Int J Androl 32:330–336. https://doi.org/10.1111/j.1365-2605.2008.00864.x
Kreda SM, Mall M, Mengos A, Rochelle L, Yankaskas J, Riordan JR, Boucher RC (2005) Characterization of wild-type and deltaF508 cystic fibrosis transmembrane regulator in human respiratory epithelia. Mol Biol Cell 16:2154–2167. https://doi.org/10.1091/mbc.E04-11-1010
Leblond CP, Clermont Y (1952) Definition of the stages of the cycle of the seminiferous epithelium in the rat. Ann N Y Acad Sci 55:548–573
Li C, Naren AP (2010) CFTR chloride channel in the apical compartments: spatiotemporal coupling to its interacting partners. Integr Biol 2:161. https://doi.org/10.1039/b924455g
Li N, Tang EI, Cheng CY (2016) Regulation of blood–testis barrier by actin binding proteins and protein kinases. Reproduction 151:R29–R41. https://doi.org/10.1530/REP-15-0463
Lishko PV, Kirichok Y, Ren D, Navarro B, Chung J-J, Clapham DE (2012) The control of male fertility by spermatozoan ion channels. Annu Rev Physiol 74:453–475. https://doi.org/10.1146/annurev-physiol-020911-153258
Mruk DD, Cheng CY (2015) The Mammalian blood-testis barrier: its biology and regulation. Endocr Rev 36:564–591. https://doi.org/10.1210/er.2014-1101
O'Donnell L, Stanton PG, Bartles JR, Robertson DM (2000) Sertoli cell ectoplasmic specializations in the seminiferous epithelium of the testosterone-suppressed adult rat. Biol Reprod 63:99–108
O'Donnell L, Nicholls PK, O'Bryan MK, McLachlan RI, Stanton PG (2011) Spermiation Spermatogenesis 1:14–35. https://doi.org/10.4161/spmg.1.1.14525
Painter RG, Valentine VG, Lanson NA, Leidal K, Zhang Q, Lombard G, Thompson C, Viswanathan A, Nauseef WM, Wang G et al (2006) CFTR expression in human neutrophils and the phagolysosomal chlorination defect in cystic fibrosis. Biochemistry 45:10260–10269. https://doi.org/10.1021/bi060490t
Potter SJ, DeFalco T (2017) Role of the testis interstitial compartment in spermatogonial stem cell function. Reproduction 153:R151–R162. https://doi.org/10.1530/REP-16-0588
Rato L, Socorro S, Cavaco JEB, Oliveira PF (2010) Tubular fluid secretion in the seminiferous epithelium: ion transporters and aquaporins in Sertoli cells. J Membr Biol 236:215–224. https://doi.org/10.1007/s00232-010-9294-x
Rato L, Alves MG, Socorro S, Duarte AI, Cavaco JE, Oliveira PF (2012) Metabolic regulation is important for spermatogenesis. Nat Rev Urol 9:330–338. https://doi.org/10.1038/nrurol.2012.77
Sorio C, Buffelli M, Angiari C, Ettorre M, Johansson J, Vezzalini M, Viviani L, Ricciardi M, Verzè G, Assael BM et al (2011) Defective CFTR expression and function are detectable in blood monocytes: development of a new blood test for cystic fibrosis. PLoS ONE 6:e22212. https://doi.org/10.1371/journal.pone.0022212

Stanton PG, Foo CFH, Rainczuk A, Stephens AN, Condina M, O'Donnell L, Weidner W, Ishikawa T, Cruickshanks L, Smith LB et al (2016) Mapping the testicular interstitial fluid proteome from normal rats. Proteomics 16:2391–2402. https://doi.org/10.1002/pmic.201600107

Waldmann R, Champigny G, Bassilana F, Voilley N, Lazdunski M (1995) Molecular cloning and functional expression of a novel amiloride-sensitive Na + channel. J Biol Chem 270:27411–27414

Zhou Q, Clarke L, Nie R, Carnes K, Lai L-W, Lien Y-HH, Verkman A, Lubahn D, Fisher JS, Katzenellenbogen BS et al. (2001) Estrogen action and male fertility: roles of the sodium/hydrogen exchanger-3 and fluid reabsorption in reproductive tract function. Proc Natl Acad Sci USA 98:14132–14137. https://doi.org/10.1073/pnas.241245898